Materials Science and Engineering A 399 (2005) 128–133

www.elsevier.com/locate/msea

Compressive behavior of wire reinforced bulk metallic glass matrix composites

Seung-Yub Lee [a], Bjørn Clausen [b], Ersan Üstündag [d,*], Haein Choi-Yim [a], C. Can Aydiner [d], Mark A.M. Bourke [c]

[a] *Department of Materials Science, M/C 138-78, California Institute of Technology, Pasadena, CA 91125, USA*
[b] *Lujan Neutron Science Center, Los Alamos National Laboratory, Los Alamos, NM 87545, USA*
[c] *Materials Science and Technology Division, Los Alamos National Laboratory, Los Alamos, NM 87545, USA*
[d] *Department of Materials Science and Engineering, Iowa State University, Ames, IA 50011, USA*

Abstract

Bulk metallic glasses (BMGs) possess a unique set of mechanical properties that make them attractive structural materials. However, when loaded without constraint, BMGs fracture catastrophically due to formation of macroscopic shear bands and this behavior reduces their reliability. To address this issue, BMG matrix composites have been developed. In this investigation, neutron diffraction was used during uniaxial compressive loading to measure the internal strains in the second phases of various BMG composites reinforced with Ta, Mo, or stainless steel wires. The diffraction data were then employed to develop a finite element model that deduced the in situ constitutive behavior of each phase. It was found that the reinforcements yielded first and started transferring load to the matrix, which remained elastic during the whole experiment. While the present composites exhibited enhanced ductility, largely due to their ductile reinforcements, they yielded at applied stresses lower than those found in W reinforced composites.

Keywords: Bulk metallic glass; Composite; Neutron diffraction; Finite element modeling; Uniaxial compression

1. Introduction

Bulk metallic glasses (BMGs) are attractive structural materials due to their unique mechanical properties: large elastic strain limit (about 2%), high strength (above 2 GPa), good fracture toughness (about 20 MPa $m^{1/2}$), good specific strength, high corrosion resistance and so on [1–3]. However, they exhibit poor ductility at room temperature as they usually fail catastrophically under unconstrained loading due to unstable shear band formation. Several BMG composites have been produced to mitigate this failure mode [4–7]. Among different kinds of composites developed, those with continuous unidirectional metallic wire reinforcements have exhibited enhanced mechanical properties. For instance, composites with Vitreloy 1 ($Zr_{41.2}Ti_{13.8}Cu_{12.5}Ni_{10.0}Be_{22.5}$) matrix and 20–80 vol.% W wires have nearly preserved the high yield strength of the BMG but have added significant ductility (total strain to fracture reaching 15–20% in compression) [5].

Our recent work using neutron diffraction (ND) and finite element modeling (FEM) has elucidated the bulk deformation mechanisms in the W wire composites [8,9]. We showed that significant thermal residual stresses develop in these composites due to the coefficient of thermal expansion (CTE) mismatch between the matrix and reinforcements [8]. Specifically, these stresses are generated during cooldown starting around the glass transition temperature of the matrix and can exceed −500 MPa in the axial direction of the W wires [8]. When the W composites are loaded in compression, these compressive thermal residual stresses induce yielding in the W wires at applied stresses lower than those expected in a residual-stress-free composite [9]. This investigation also showed that it is always the W wires that first experience plastic deformation followed by “yielding” in the BMG matrix in the form of multiple shear band formation [9]. The presence of the W wires stabilizes the production of multiple shear bands in the

* Corresponding author. Tel.: +1 515 294 9678; fax: +1 515 294 7202.
E-mail address: ustundag@iastate.edu (E. Üstündag).

0921-5093/$ – see front matter © 2005 Elsevier B.V. All rights reserved.
doi:10.1016/j.msea.2005.02.032

Table 1
Properties of reinforcement wires and two BMG matrices: $Zr_{57}Nb_5Al_{10}Cu_{15.4}Ni_{12.6}$ (Vit. 106) and $Zr_{41.2}Ti_{13.8}Cu_{12.5}Ni_{10.0}Be_{22.5}$ (Vit. 1)

	Elastic modulus (E) (GPa)	Poisson's ratio (ν)	Yield strength, (σ_Y) (MPa)	CTE ($10^{-6}\,K^{-1}$)
Vit. 106	85 [17]	0.38 [17]	1800 [17]	8.7 [17] (at 293 K)
Type 302 SS	193 [15]	0.25 [15]	250 [15]	17.2–18.4 [15] (at 293–800 K)
Mo	330 [18]	0.38 [18]	400 [18]	4.8–5.7 [16] (at 293–800 K)
Ta	186 [17]	0.35 [17]	350 [17]	6.3–7.2 [16] (at 293–800 K)
Vit. 1 [9]	96	0.36	1900	9.0 (at 293 K)
W [9]	410	0.28	1300	4.5 (at 293 K)

BMG thereby enhancing the overall ductility of the composite.

A similar combined ND–FEM methodology is followed here. A different BMG alloy, Vitreloy 106 ($Zr_{57}Nb_5Al_{10}Cu_{15.4}Ni_{12.6}$) was chosen as the matrix. Vit. 106 is among the best glass forming alloys, i.e., can be cast into large dimensions and is Be-free, an important environmental advantage. Three different materials were considered for reinforcement: type 302 stainless steel (SS), Mo and Ta. The reinforcement volume fraction was kept at 40%, and similar to the W composites, the wires were unidirectional. These reinforcements have different properties compared to W (Table 1). For instance, their yield strengths and Young's moduli are lower than those of W and one of them (steel) has a higher CTE than that of the matrix. The purpose of the present study is to quantify the effects of the different reinforcement properties on the deformation of the BMG composites.

2. Experimental procedure

Ingots of the Vit. 106 alloy were prepared by arc-melting elemental metals with the purity of 99.7% or higher in a Ti-gettered Ar atmosphere. Stainless steel (type 302) and Mo reinforcement wires were purchased from Thermionic, Inc. (North Plainfield, NJ 07060) and Alfa Aesar (Ward Hill, MA 01835) supplied the Ta wire. All wires were 0.25 mm in diameter and were straightened before processing the composites using the melt infiltration procedure [10]. Specifically, a stainless steel tube containing the wire bundle at the bottom was evacuated to about 3×10^{-2} Torr and flushed with Ar gas several times. While still under vacuum, it was heated to 975 °C and held there for 10 min to melt the Vit. 106 alloy. After melting the metallic glass, the temperature was lowered to 875 °C and held for another 15 min during which 100 psi Ar gas pressure was applied to force the molten alloy into the tube. This was followed by quenching the tube in water at room temperature. Test samples were machined into a cylindrical geometry of 6 mm diameter and 14.4 mm length with the fiber axes parallel to the sample axis.

Neutron diffraction experiments were conducted under uniaxial compression using the SMARTS diffractometer [11] at the Lujan Neutron Science Center, Los Alamos National Laboratory. The geometric setup of SMARTS allows simultaneous measurements in longitudinal and transverse directions. The diffraction data were collected using the time-of-flight technique. Elastic strain in the wires was calculated from changes in their lattice parameters as a function of applied stress. Strains are reported relative to the initial strain state at a −5 MPa applied stress (which was needed to hold samples in a horizontal loading geometry). The lattice parameters were determined from the entire diffraction pattern to within a 5×10^{-5} fitting error using the Rietveld method [12,13]. Additional details about the Rietveld analysis can be found in [8]. Each composite was subjected to several loading-unloading cycles while the longitudinal macroscopic strain was measured with an extensometer. Neutron data were collected under load control in 15–20 min runs at approximately 25–100 MPa stress intervals. A compressive strain rate of about $10^{-4}\,s^{-1}$ was employed between load levels.

3. Finite element modeling

Neutron diffraction measurements only record the elastic (lattice) strains; therefore, for a comprehensive interpretation of the composite's deformation, a mechanics model is required. This model is especially essential in this study because the diffraction data are limited to the crystalline wires and measurement of the BMG matrix is not possible due to its amorphous structure. A finite element model was developed for this purpose using the commercial software ABAQUS™ [14]. A three-dimensional mesh was employed to allow loading parallel to the fiber axis (Fig. 1). The plane strain assumption was utilized in the model by constraining planes that are perpendicular to the fiber axis to remain planar (Fig. 1). Therefore, the model addresses behavior deep beneath the surface of the sample and does not account for surface effects. The calculations employed a unit cell model, and symmetry boundary conditions were imposed on all outer surfaces. Due to the cylindrical shape of the fiber, second order, 20 node, brick elements were used in the mesh, and reduced integration points were employed for speedy calculations. For comparison with the diffraction data which average across the sample cross-section, the volume average of elastic strains were calculated for the two phases using the element volume and the "element centroid" value [14] of the elastic strain at each element.

The material parameters used in the calculations are shown in Table 1. Table 2 exhibits the information obtained from the FE calculations. The thermal residual stresses were calculated assuming they are generated starting at the glass tran-

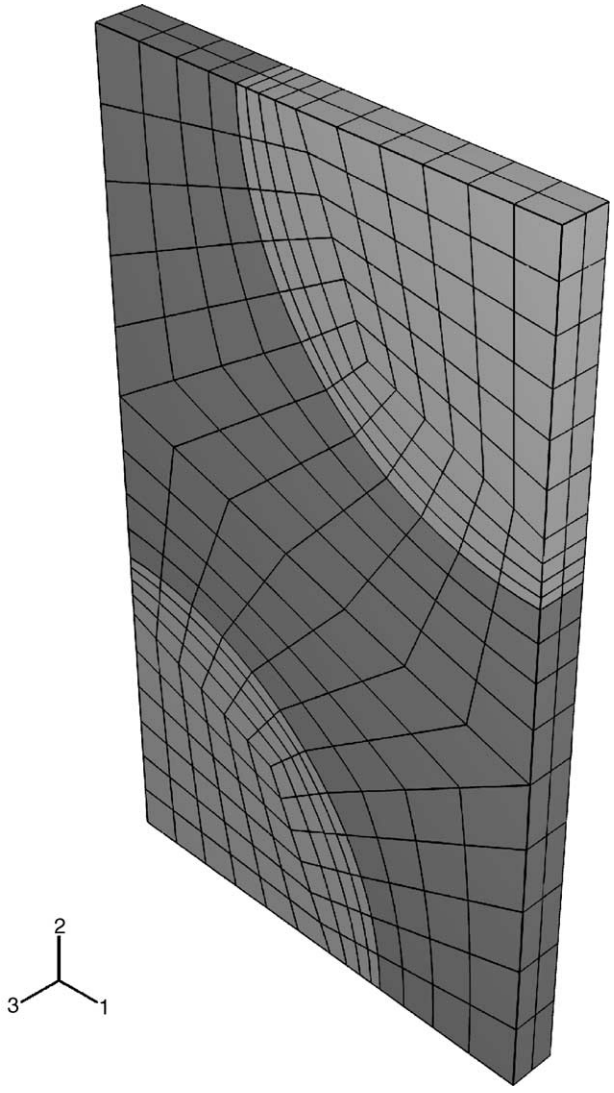

Fig. 1. Mesh used in the FEM calculations for a 40% fiber model. The light gray elements represent the fibers while the dark gray elements represent the matrix. The surfaces in the 1–2 planes (perpendicular to the fiber axis) are constrained to remain planar, effectively imposing a plane strain behavior. Loading is applied along direction 3.

sition of Vit. 106 (∼414 °C) [19]. Our previous work [9] has shown that in a composite both the reinforcements and the matrix exhibit a different constitutive behavior than their monolithic forms. Therefore, the in situ yielding and hardening behavior were treated as variables to optimize the agreement between the model and the experimental data (both lattice strain in the wires—from ND, and macroscopic strain in the composite—from the extensometer). The FE model employed the kinematic hardening assumption [14] for the wire constitutive behavior to recalculate their hardening during unloading and to account for the reversed yielding observed in the reinforcements upon unloading. The BMG appeared to remain elastic throughout the whole experiment for all three composites and its yield point was determined to be the same as that in literature (1800 MPa). The fitted values for the in situ yield strengths of the wires, however, did change inside composites and are shown in Table 2. The estimated error bars for these fits are about 5%. The resulting phase dependent, in situ stress–strain plots are shown in Fig. 2. The reader should note that these plots represent a reasonable solution based on the available data and the assumptions employed in the FEM, but are not necessarily unique in a strict mathematical sense.

Table 2
Properties of 40% wire reinforced BMG composites *calculated* using FEM in comparison with neutron diffraction data

	Wire yield strength (von Mises stress, σ_Y) (MPa)	Wire axial thermal residual stress (MPa)	Composite axial yield stress (MPa)
Type 302 SS	175	∼0	−20
Mo	350	−160	−140
Ta	80	−90	−20
W [9]	1300	−300	−600

The data in the last row were obtained in a previous study [9].

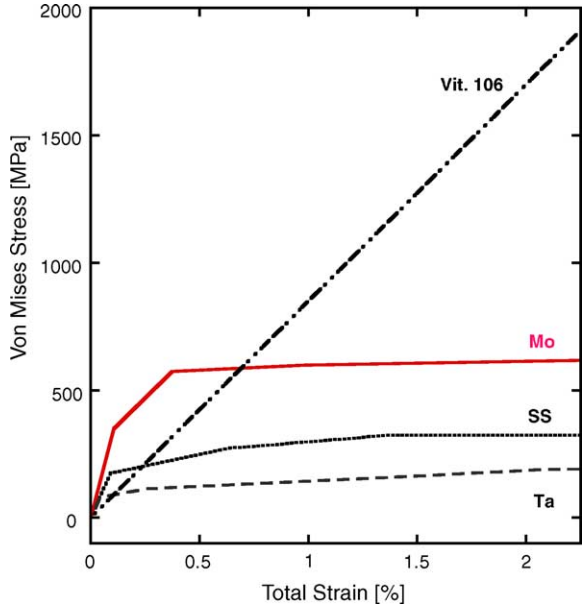

Fig. 2. In situ stress–strain behavior for each phase as calculated by the finite element model. These plots were deduced by comparing the experimental data with model predictions.

4. Results and discussion

Figs. 3–5 exhibit the experimental data in comparison with model predictions. The stress–strain plots shown in Fig. 2 for each phase were deduced as a result of this comparison. As shown in the Table 1, since the thermal expansion coefficients of Mo and Ta are smaller than that of the matrix, the Mo and Ta wires are expected to be under compressive stress following sample processing while the BMG experiences tensile axial and hoop stress and compressive radial stress. This residual stress state is predicted to be reversed in the stainless steel

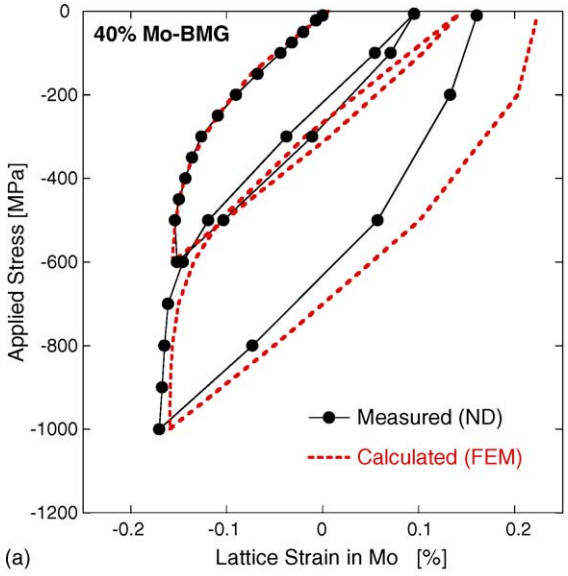

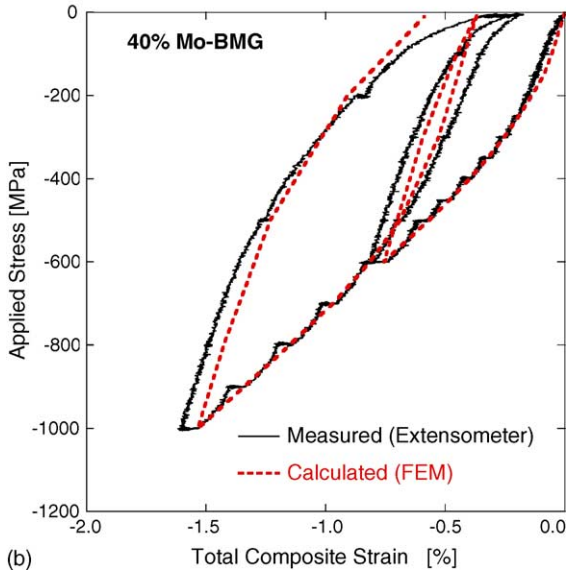

Fig. 3. Neutron (a) and macroscopic composite data (b) of the 40% Mo—Vit. 106 matrix composite compared with the predictions of the FEM model.

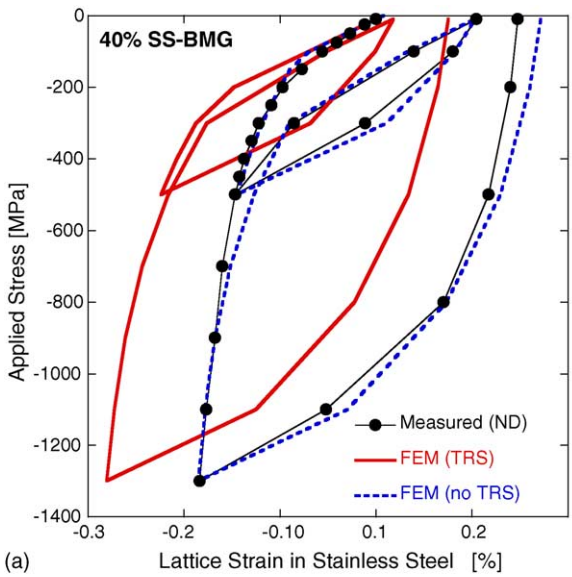

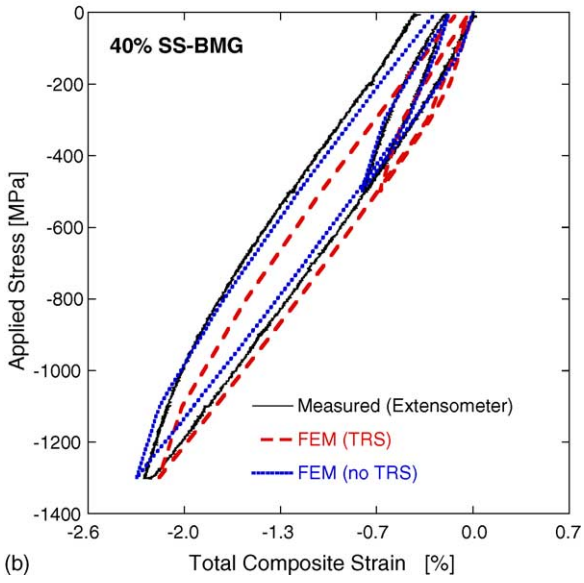

Fig. 4. Neutron (a) and macroscopic composite data (b) of the 40% SS (type 302)—Vit. 106 matrix composite compared with the predictions of the FEM model. Two versions of the model are shown: the first version ("TRS") includes thermal residual stresses while the second one assumes there are no thermal residual stresses ("no TRS").

composite because of an opposite CTE mismatch between the wires and matrix.

Due to lack of proper stress-free reference wires, the thermal residual stresses could not be measured in this study. However, the values calculated (see Table 2) based on the assumption that stress buildup starts at the BMG glass transition temperature [8,9] provided reasonable approximations when ND data from loading experiments were compared to model predictions except for the SS composite. The model fits for this composite that included calculated thermal residual stresses were not as satisfactory as those that disregarded such stresses (Fig. 4). It was therefore concluded that the thermal residual stresses were largely relaxed in the SS/BG composite. One possible explanation for this behavior is that the SS/BMG interface in these composites has generally been observed to be weaker than that found in W, Mo and Ta reinforced BMG composites [20]. The predicted tensile radial residual stress at the SS/BMG interface may have aided the relaxation process and even experienced debonding during cooling.

A comparison of FE model predictions and the experimental data suggests that the model is successful in describing the early part of the deformation of all composites and is especially satisfactory for the SS/BMG composite (Figs. 3–5). In all composites, the wires appear to yield first while the BMG matrix remains elastic throughout the whole deformation (Fig. 2). The wires also yield during unloading as indi-

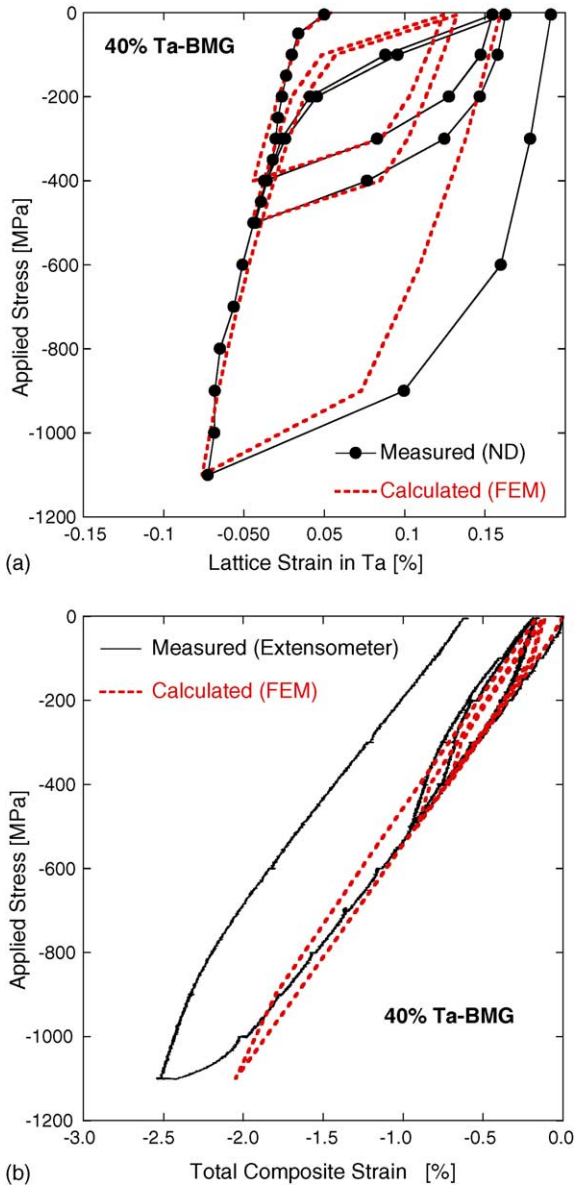

Fig. 5. Neutron (a) and macroscopic composite data (b) of the 40% Ta—Vit. 106 matrix composite compared with the predictions of the FEM model.

cated by the non-linear unloading curves. Another interesting observation based on the constitutive behaviors presented here (see Fig. 2) is that, compared to literature data, the in situ yield strength of the wires has decreased in all three composites (Table 2). The decrease is especially pronounced in the Ta wires whose yield strength dropped from 350 MPa to about 80 MPa (compare Tables 1 and 2). This can be attributed to a probable annealing of the wires during composite processing, a phenomenon also seen in W/BMG composites [9].

Compared to W reinforced BMG composites, those reinforced with SS, Mo and Ta wires exhibit much lower yield strengths in compression. Forty percent W/BMG composites started yielding at around −600 MPa [9] (see Table 2). In comparison, the axial yield stress in the present composites is −120 MPa for SS, −140 MPa for Mo and −20 MPa for Ta composites (Table 2). These values are quite low and suggest that the present composites are not as attractive as those with W wires. Nevertheless, they do enhance the ductility of the BMG matrix and prevent the formation of unstable shear bands [20]. It is also worth noting that due to their much higher Young's modulus (Table 1), the SS, Mo and Ta wires carry a higher proportion of the applied stress compared to the BMG matrix and delay the latter's yielding.

5. Conclusions

In an attempt to develop bulk metallic glass composites with enhanced ductility, stainless steel, Mo and Ta wires were incorporated in a BMG matrix via a melt infiltration process. The deformation of the three composites under uniaxial compression was studied using an integrated neutron diffraction and finite element (FE) approach. The FE model yielded a reasonable version of in situ stress–strain plots for both reinforcements and the matrix. It was found that the reinforcements yielded first and started transferring load to the matrix, which remained elastic throughout the whole experiment. The reinforcements were seen to possess yield strengths lower than their monolithic forms, likely due to annealing during processing. After optimizing material properties to fir experimental data, the FE model developed was reasonably successful in describing both the macroscopic composite deformation and the lattice strain evolution in the reinforcements.

Acknowledgements

This study is supported by the National Science Foundation (MRSEC program, DMR-0080065 and CAREER Award DMR-9985264). Lujan Neutron Science Center is a national user facility funded by the United States Department of Energy, Office of Basic Energy Sciences, under contract number W-7405-ENG-36.

References

[1] C.J. Gilbert, R.O. Ritchie, W.L. Johnson, Appl. Phys. Lett. 71 (1997) 476.
[2] W.L. Johnson, JOM J. Miner. Met. Mater. Soc. 54 (2002) 40.
[3] H.A. Bruck, T. Christman, A.J. Rosakis, W.L. Johnson, Scripta Metall. 30 (1994) 429.
[4] R.D. Conner, R.B. Dandliker, V. Scruggs, W.L. Johnson, Int. J. Impact. Eng. 24 (2000) 435.
[5] R.D. Conner, R.B. Dandliker, W.L. Johnson, Acta Mater. 46 (1998) 6089.
[6] H. Choi-Yim, W.L. Johnson, Appl. Phys. Lett. 71 (1997) 3808.
[7] H. Choi-Yim, R. Busch, U. Köster, W.L. Johnson, Acta Mater. 47 (1999) 2455.
[8] D. Dragoi, E. Üstündag, B. Clausen, M.A.M. Bourke, Scripta Mater. 45 (2001) 245.

[9] B. Clausen, S.-Y. Lee, E. Üstündag, C.C. Aydiner, R.D. Conner, M.A.M. Bourke, Scripta Mater. 49 (2003) 123.
[10] R.B. Dandliker, R.D. Corner, W.L. Johnson, J. Mater. Res. 13 (1998) 2896.
[11] M.A.M. Bourke, D.C. Dunand, E. Üstündag, Appl. Phys. A 74 (2002) 1707.
[12] H.M. Rietveld, Acta Cryst. 22 (1967) 151.
[13] A.C. Larson, R.B. Von Dreele, GSAS-General Structure Analysis System, LAUR 86-748: Los Alamos National Laboratory, 1986.
[14] ABAQUS, Standard User's Manual, Version 6.3, Hibbitt, Karlsson & Sorensen, Inc., 2002.
[15] H.E. Boyer, T.L. Gall, Handbook of Stainless Steels, American Society for Metals, New York, NY, 1977, pp. 7–19.
[16] Y.S. Touloukian, R.K. Kirby, R.E. Taylor, P.D. Desai, Thermophysical properties of matter Thermal Expansion, Metallic Elements and Alloys, vol. 12, IFI/Plenum, New York, NY, 1977, pp. 208, 316, 354.
[17] H. Choi-Yim, R.D. Conner, W.L. Johnson, Ann. Chim. Sci. Mater. 27 (2002) 113.
[18] D.R. Lide, Handbook of Chemistry and Physics, 82nd ed., CRC Press, Boca Raton, FL, 2001, pp. 12–220.
[19] J.F. Löffler, S. Bossuyt, S.C. Glade, W.L. Johnson, W. Wagner, P. Thiyagarajan, Appl. Phys. Lett. 77 (2000) 525.
[20] S.-Y. Lee, H. Choi-Yim, E. Üstündag, unpublished research, 2002.